

Broken degeneracies: the rotation curve and velocity anisotropy of the Milky Way halo

A. J. Deason^{1*}, V. Belokurov¹, N. W. Evans¹ and J. H. An²

¹*Institute of Astronomy, Madingley Rd, Cambridge, CB3 0HA*

²*National Astronomical Observatories, Chinese Academy of Sciences, A20 Datun Road, Chaoyang District, Beijing 100012, PR China*

May 2012

ABSTRACT

We use distant Blue Horizontal Branch stars with Galactocentric distances $16 \text{ kpc} < r < 48 \text{ kpc}$ as kinematic tracers of the Milky Way dark halo. We model the tracer density as an oblate, power-law embedded within a spherical power-law potential. Using a distribution function method, we estimate the overall power-law potential and the velocity anisotropy of the halo tracers. We measure the slope of the potential to be $\gamma \sim 0.4$ and the overall mass within 50 kpc is $\sim 4 \times 10^{11} M_{\odot}$. The tracer velocity anisotropy is radially biased with $\beta \sim 0.5$, which is in good agreement with local solar neighbourhood studies. Our results provide an accurate outer circular velocity profile for the Milky Way and suggest a relatively high concentration dark matter halo ($c_{\text{vir}} \sim 20$).

Key words: Galaxy: halo — Galaxy: kinematics and dynamics — dark matter — Stars — horizontal branch

1 INTRODUCTION

The mass of our Galaxy is a fundamental – yet poorly constrained – astrophysical quantity. Several attempts have been made to measure the total mass of the Milky Way using kinematic tracers (e.g. Wilkinson & Evans 1999; Xue et al. 2008; Gnedin et al. 2010; Watkins et al. 2010), the orbits of the Magellanic Clouds (e.g. Lin & Lynden-Bell 1982; Besla et al. 2007), the local escape speed (Smith et al. 2007), and the timing argument (Li & White 2008). The results of this extensive list of work is distressingly inconclusive with total masses ranging from $0.5 - 3 \times 10^{12} M_{\odot}$.

The most common method to probe the mass distribution is to use kinematic tracers such as globular clusters, stellar halo stars and satellite galaxies. The properties of these tracer populations are linked to the underlying matter distribution via the steady state (spherical) Jeans equation:

$$M(< r) = \frac{r\sigma_r^2}{G} \left(-\frac{d\ln\rho_{\text{tr}}}{d\ln r} - \frac{d\ln\sigma_r^2}{d\ln r} - 2\beta \right) \quad (1)$$

At face value, this equation is remarkably simple; the mass distribution is related to the logarithmic gradients of the radial velocity dispersion σ_r and density (ρ_{tr}) of the tracers, as well as the velocity anisotropy (β). Without firm knowledge of the tracer properties, our Galactic mass measures suffer from the well-known *mass-anisotropy-density* degeneracy.

The density distribution of the stellar halo has been studied extensively (e.g. Yanny et al. 2000; Chen et al. 2001; Newberg & Yanny 2006; Jurić et al. 2008). However, only in recent

years has a consensus on the profile been reached (e.g. Sesar et al. 2011; Deason et al. 2011b). Our knowledge of the orbital properties of the stellar halo stars is limited to the solar neighbourhood where the velocity ellipsoid is radially biased (e.g. Képley et al. 2007; Smith et al. 009a; Bond et al. 2010). In contrast, Sirko et al. (2004) inferred the velocity anisotropy of stellar halo stars at larger distances (i.e. $r > 10 \text{ kpc}$) from line-of-sight velocities alone, and found an *isotropic* velocity ellipsoid; this is in contrast to the strongly radial anisotropy found locally. However, the uncertainties in these measurements proved too large for a conclusive result.

In this *Letter*, we break the mass-anisotropy-density degeneracy for the first time. We adopt the recently measured stellar halo density of Deason et al. (2011b) and disentangle the remaining mass-anisotropy degeneracy using line-of-sight velocities of Blue Horizontal Branch tracers out to $r \sim 50 \text{ kpc}$ selected from the Sloan Digital Sky Survey (SDSS). Several studies have measured the *total* mass of the Galaxy within $r \sim 50 \text{ kpc}$ (e.g. Kochanek 1996; Wilkinson & Evans 1999; Sakamoto et al. 2003; Xue et al. 2008) but the mass profile is poorly known. We measure the slope of the overall potential and thus provide an accurate circular velocity profile out to 50 kpc.

2 METHOD

Beyond the solar neighbourhood, we typically have full spatial information for stellar halo stars together with accurate line-of-sight velocities. While the density distribution of stellar halo stars has been extensively studied, there have been very few attempts to infer the velocity anisotropy. In the absence of information on the proper

* E-mail: ajd75,vasily,nwe@ast.cam.ac.uk,jinan@nao.cas.cn

motions, most previous studies have resorted to assuming a velocity anisotropy for the tracers. Often, this assumption is motivated by the predictions of cosmological simulations (e.g. Xue et al. 2008; Gnedin et al. 2010). However, the line-of-sight velocity distribution (LOSVD) itself contains valuable kinematic evidence that is often not suitably exploited. For example, information on the velocity anisotropy is encoded within the fourth order moments of the LOSVD (i.e. the kurtosis; see e.g. Figure 3 of Deason et al. 2011a). There are two main requirements needed to extract such information from the LOSVD: i) a large sample of tracers and ii) tracers with a wide sky coverage.

2.1 Halo Tracers: Blue Horizontal Branch Stars

The Sloan Digital Sky Survey (SDSS) has now mapped an impressive 20,000 deg² of sky. Furthermore, the dedicated spectroscopic Sloan Extension for Galactic Understanding and Exploration (SEGUE) survey has unearthed several thousand kinematic tracers of the stellar halo. In particular, ~ 4000 Blue Horizontal Branch (BHB) stars have been spectroscopically identified out to $r < 60$ kpc (Xue et al. 2011). BHB stars are excellent halo tracers owing to their intrinsic brightness ($M_g \sim 0.5$) and accurate distance estimates ($\Delta M_g \sim 0.15$). The combination of wide sky coverage plus a large sample of distant halo tracers provides a unique opportunity to break the mass-anisotropy-density degeneracy in the halo. In fact, the density profile of these tracers has recently been measured by Deason et al. (2011b) (hereafter, DBE) using the latest photometric SDSS DR8 release. They found that the stellar halo out to $r \sim 50$ kpc is well-described by a smooth flattened density distribution of broken power-law form:

$$\rho(r_q) \propto \begin{cases} r_q^{-2.3} & r_q \leq 27 \text{ kpc}, \\ r_q^{-4.6} & r_q > 27 \text{ kpc}, \end{cases} \quad (2)$$

with $r_q^2 = R^2 + z^2/q^2$, where the minor-axis to major-axis ratio is $q = 0.59$. Armed with this independent measure of the density profile, a large kinematic sample of BHB stars can be used to constrain their velocity anisotropy *and* the underlying mass distribution. To this end, we use BHB stars selected from the SDSS DR8 spectroscopic survey by Xue et al. (2011). We assign distances using the colour-absolute magnitude relation derived in DBE. For simplicity, we only consider stars beyond the ellipsoidal break radius, $r_q = 27$ kpc (corresponding to spherical radii $r \gtrsim 16 - 26$ kpc). This ensures that the tracers are far away from the disc of the Galaxy, and allows us to model the density distribution of the tracers with a single power-law. The final sample consists of 1933 stars with Galactocentric radii in the range $16 < r/\text{kpc} < 48$. Observed heliocentric velocities are converted to Galactocentric ones by assuming a circular speed¹ of 240 km s⁻¹ at the position of the sun ($R_0 = 8.5$ kpc) with a solar peculiar motion $(U, V, W) = (11.1, 12.24, 7.25)$ km s⁻¹. Here, U is directed toward the Galactic centre, V is positive in the direction of Galactic rotation and W is positive towards the North Galactic Pole. In Fig. 1, we show the final sample of 1933 BHB stars in the (x, z) plane (left panel) and their line-of-sight velocities as a function of radius (right panel).

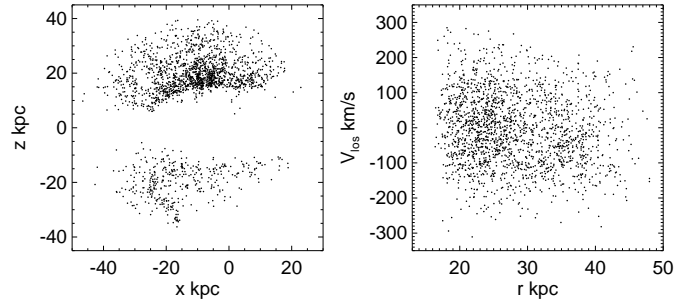


Figure 1. Left panel: The spatial distribution of BHB stars in the x - z plane with $r_q > 27$ kpc. Right panel: The line-of-sight velocities as a function of Galactocentric radius.

| α, q | γ | Φ_0 $10^5 \text{ km}^2 \text{ s}^{-2}$ | β | $M(< 50 \text{ kpc})$ $10^{11} M_\odot$ |
|-------------|------------------------|--|----------------------|--|
| 4.6, 0.59 | $0.4^{+0.04}_{-0.15}$ | $4^{+0.5}_{-0.5}$ | $0.5^{+0.08}_{-0.2}$ | $4.2^{+0.4}_{-0.4}$ |
| 4.6, 1.0 | $0.35^{+0.1}_{-0.18}$ | $4^{+0.6}_{-0.5}$ | $0.4^{+0.15}_{-0.2}$ | $4.4^{+0.5}_{-0.5}$ |
| 3.5, 1.0 | $0.35^{+0.08}_{-0.17}$ | $3^{+0.5}_{-0.5}$ | $0.4^{+0.1}_{-0.2}$ | $3.3^{+0.4}_{-0.4}$ |

Table 1. The results of the maximum likelihood analysis. The tracer density parameters (α, q) are fixed.

2.2 Distribution Functions for Spherical and Flattened Tracers

We model the dynamical properties of the BHB tracers using a distribution function (DF) method (see e.g. Binney & Tremaine 2008 and references therein). The phase-space structure of dynamical tracers is described by a probability density function; this is often a more practical approach than following individual orbits.

We always assume that the overall potential is spherically symmetric, as suggested by several recent studies (e.g. Smith et al. 009b, Koposov et al. 2010, Agnello & Evans 2012). As we are restricting attention to stars beyond 16 kpc from the Galactic centre, we can safely ignore any flattening influence provided by the Galactic disc. For simplicity, we use a power-law profile for the potential $\Phi = \Phi_0 (r/1 \text{ kpc})^{-\gamma}$, where γ is constant.

We investigate models in which the stellar halo density is a spherical power-law, namely $\rho \propto r^{-\alpha}$ with γ constant. The DFs have been described elsewhere (e.g. Evans et al. 1997; An & Evans 2006; Deason et al. 2011a). The velocity distribution is given in terms of the binding energy $E = \Phi(r) - \frac{1}{2}(v_l^2 + v_b^2 + v_{\text{los}}^2)$ and the total angular momentum $L = \sqrt{L_x^2 + L_y^2 + L_z^2}$ as

$$F(E, L) \propto L^{-2\beta} f(E) \quad (3)$$

where

$$f(E) = E^{\beta(\gamma-2)/\gamma + \alpha/\gamma - 3/2} \quad (4)$$

Here, β is the Binney anisotropy parameter defined as $\beta = 1 - \frac{1}{2}(\langle v_\theta^2 \rangle + \langle v_\phi^2 \rangle) / \langle v_r^2 \rangle$, and taken as constant.

We also investigate models in which the stellar halo density is a power-law, but with constant flattening q , as suggested by a number of recent studies (e.g. DBE, Sesar et al. 2011). The extension of eqns (3)-(4) into the flattened regime is given by (see e.g.,

¹ Note that we adopt the recently revised LSR (e.g. Reid et al. 2009; McMillan 2011) but our main results are unchanged if we use the conventional value of 220 km s⁻¹.

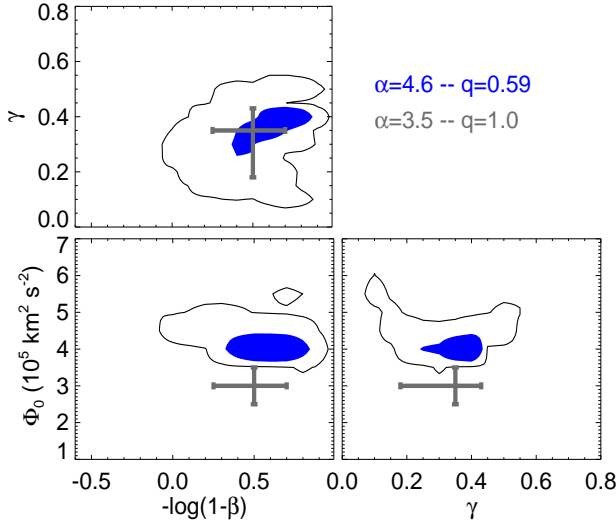


Figure 2. The likelihood contour levels for the BHB stars assuming the DBE density profile. The blue shaded regions show the 1σ (68%) confidence region, whilst the solid lines encompass the 2σ (95%) confidence region. The gray arrows indicate the confidence regions when a spherical tracer density is assumed with slope of 3.5. The assumption of a shallower tracer density profile leads to a bias towards lower masses.

de Bruijne et al. 1996)

$$F(E, L^2, L_z^2/L^2) \propto L^{-2\beta} f(E) h(e^2 L_z^2/L^2) \quad (5)$$

where

$$\begin{aligned} h(e^2 L_z^2/L^2) &= \sum_{k=0}^{\infty} \frac{(1)_k \left(\frac{\alpha}{2}\right)_k}{k! \left(\frac{1}{2}\right)_k} (e^2 L_z^2/L^2)^k \\ &= {}_2F_1\left(1, \frac{\alpha}{2}; \frac{1}{2}; e^2 L_z^2/L^2\right). \end{aligned} \quad (6)$$

Here, $e = \sqrt{1 - q^2}$ is the eccentricity, $(\dots)_k$ is Pochhammer's symbol where $(x)_k = \Gamma(x+k)/\Gamma(x)$ and ${}_2F_1$ is a hypergeometric function. Remarkably, the effect of flattening is provided by a simple multiplicative factor.

In our analysis, we assume that the tracer density, described by α and q , is known. Our favoured model is the single-power law for $r_q > 27$ kpc found by DBE, in which $\alpha = 4.6$ and $q = 0.59$. However, we also consider the spherical limit of this density (i.e. $q = 1, \alpha = 4.6$) and the commonly used spherical density with a power-law slope of $\alpha = 3.5$. These latter two examples illustrate the biases caused when an incorrect tracer density is adopted. Note that we ignore rotation in this analysis as previous work has inferred that the overall rotation signal is negligible for the stellar halo (Deason et al. 2011a).

3 RESULTS

Our aim is to constrain the overall potential (defined by the slope and normalisation) and tracer velocity anisotropy. We have full 3D spatial information for the tracers, but only have one velocity component. The LOSVD is constructed by marginalising over the unknown tangential components and a maximum-likelihood method

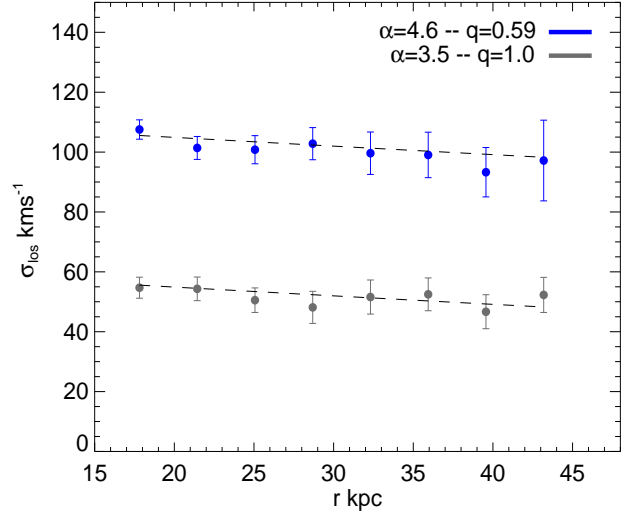


Figure 3. The line-of-sight velocity dispersion profile of the maximum likelihood models when a DBE density distribution is assumed (blue points) and when a spherical power-law profile with index 3.5 is assumed (gray points, offset by -50 km s^{-1}). The dashed line shows the fit to the BHB data derived by Xue et al. (2008). In each case, 2000 stars are drawn at random from the maximum likelihood function. The same line-of-sight velocity dispersion profile can be reproduced by either model, even though they have very different mass profiles.

is used to derive the unknown parameters, Φ_0 , γ and β :

$$L(\Phi_0, \gamma, \beta) = \sum_{i=1}^N \log F_{\text{los}}(l_i, b_i, d_i, v_{\text{los}_i}, \Phi_0, \gamma, \beta), \quad (7)$$

Here, F_{los} is the LOSVD (see e.g. equation 7 in Deason et al. 2011a) and N is the total number of BHB star tracers in our sample. The likelihood confidence contours are shown in Fig. 2 when our favoured ($\alpha = 4.6, q = 0.59$) tracer density is adopted. The blue shaded region indicates the 1σ confidence region whilst the solid black line gives the 2σ confidence region. For comparison, the gray error bars show the 1σ confidence region when a spherical tracer density is assumed with slope 3.5, which is a widely assumed value in the literature (e.g. Xue et al. 2008; Deason et al. 2011a). Our results favour a radially biased velocity anisotropy with $\beta = 0.5^{+0.08}_{-0.2}$; this is the most accurate measure of the velocity anisotropy beyond the solar neighbourhood from line-of-sight velocities alone. Somewhat surprisingly, our measurement is in good agreement with local solar neighbourhood constraints on the velocity ellipsoid (e.g. Kepley et al. 2007; Smith et al. 2009a; Bond et al. 2010). This suggests that the velocity anisotropy of stellar halo stars may be approximately *constant* over a large radial range. In addition, we note that a radially biased velocity anisotropy of $\beta \sim 0.5$ is in good agreement with the predictions of cosmological simulations (e.g. Diemand et al. 2007; Sales et al. 2007; Navarro et al. 2010). Our results are also consistent (within the errors) with the velocity ellipsoid measured by Sirko et al. (2004). While these authors favour an isotropic ellipsoid, the errors in the tangential components are large and also allow for radial anisotropy.

This methodology also allows us to measure simultaneously the normalisation and slope of the potential, the latter of which has not been previously measured for our Galaxy. We measure the overall slope of the potential to be $\gamma = 0.4^{+0.04}_{-0.15}$. The mass enclosed

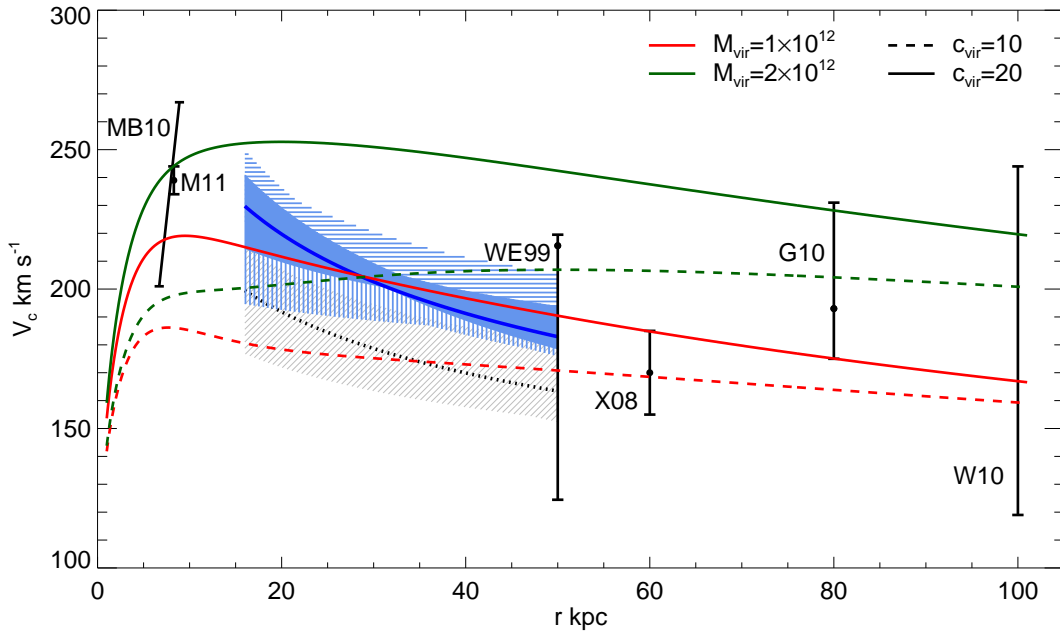


Figure 4. The circular velocity profile of the Galaxy. The blue shaded region shows the 1σ constraint found in this work for our favoured tracer density profile of DBE. The blue vertical and horizontal line-filled regions indicate the additional uncertainty with systematic errors in the tracer density power-law index of ± 0.2 dex. The gray line-filled region shows the profile when instead a spherical tracer density with power-law index 3.5 is used. The solid and dotted lines indicate the maximum likelihood solutions. Constraints on the circular velocity from other studies are shown by the black error bars: McMillan & Binney 2010 (MB10; Solar neighbourhood), McMillan 2011 (M11; Solar neighbourhood), Wilkinson & Evans 1999 (WE99; $r = 50$ kpc), Xue et al. 2008 (X08; $r = 60$ kpc), Gnedin et al. 2010 (G10; $r = 80$ kpc), Watkins et al. 2010 (W10; $r = 100$ kpc). The solid/dashed red and green curves show models with dark matter components of NFW form and a baryonic component consisting of an exponential disk with mass $5 \times 10^{10} M_\odot$ and scale length 3 kpc and a Hernquist bulge with mass $5 \times 10^9 M_\odot$. A dark matter component with virial mass $M_{\text{vir}} \sim 10^{12} M_\odot$ and concentration $c_{\text{vir}} \sim 20$ is favoured by the results of this study.

within $r = 50$ kpc is $M(50) = 4.2 \pm 0.4 \times 10^{11} M_\odot$; in good agreement with independent mass measures out to this radius (Kochanek 1996: $M(50) = 4.9^{+1.1}_{-1.1} \times 10^{11} M_\odot$, Wilkinson & Evans 1999: $M(50) = 5.4^{+0.2}_{-3.6} \times 10^{11} M_\odot$, Sakamoto et al. 2003: $M(50) = 5.5^{+0.1}_{-0.4} \times 10^{11} M_\odot$, Smith et al. 2007: $M(50) = 3.6 - 4.0 \times 10^{11} M_\odot$, Besla et al. 2007: $M(50) \sim 4.5 \times 10^{11} M_\odot$).

In Table 1, we give the maximum likelihood solutions when different tracer density profiles are adopted. The differences are modest when a spherical tracer population is assumed; the velocity anisotropy is less radially biased and the potential slope is slightly shallower. On the other hand, adopting a shallower tracer density slope (i.e. $\alpha = 3.5$) leads to significant differences in the total mass; the mass is 30% higher when the tracer density profile of our favoured model ($\alpha = 4.6$) is assumed instead of the more commonly adopted $\alpha = 3.5$.

In Fig. 3, we show the line-of-sight velocity dispersion profile of our maximum likelihood solutions. We draw 2000 stars from the appropriate distribution function using a Monte-Carlo method; the blue and gray points show the resulting line-of-sight velocity dispersions for the DBE ($\alpha = 4.6$, $q = 0.59$) and spherical comparison ($\alpha = 3.5$) density models respectively. The gray points are offset by -50 km s^{-1} for illustrative purposes. The dashed line shows a fit to the observed relation for BHB stars derived by Xue et al. (2008). This plot highlights the degeneracy between different density models; both are able to reproduce the observed line-of-sight velocity distribution but they give very different mass profiles.

3.1 Milky Way Circular Velocity Profile

In Fig. 4, we show the circular velocity profile of the Galaxy derived from our model. The blue shaded region shows the 1σ confidence region from this work assuming a DBE density profile with slope $\alpha = 4.6$ and flattening $q = 0.59^2$. We also consider systematic uncertainties of 0.2 dex in the tracer density slope. Note that we do not consider systematic uncertainties in the flattening of the tracer density profile, as the mass profile is much more sensitive to changes in the power-law index of the tracer density (e.g. see Table 1). DBE found statistical errors of $\sim 0.1 - 0.2$ dex in the power-law indices and systematic effects due to the presence of un-relaxed substructure can also cause biases of $\sim 0.2 - 0.3$ dex. The blue line-filled regions indicate the additional uncertainties that could be caused by such biases. The normalisation of the circular velocity is slightly increased or decreased when the tracer density is modified upwards or downwards by 0.2 dex. However, the overall potential slope and tracer velocity anisotropy are hardly changed. This emphasises that an *accurate* measure of the tracer density profile is vital to infer the mass profile of our Galaxy. The hatched gray region gives the mass profile when a spherical density profile with slope $\alpha = 3.5$ is assumed instead. The points with error bars show other constraints from the literature.

The green and red lines show model profiles assuming a baryonic component consisting of a (spherically averaged) exponen-

² We note that our assumption of a single power-law for the overall potential is most uncertain at the end points of our radial range (i.e. $r \lesssim 20$ kpc or $r \gtrsim 45$ kpc).

tial disc³ with mass $5 \times 10^{10} M_{\odot}$ and scale length 3 kpc and Hernquist bulge with mass $5 \times 10^9 M_{\odot}$ (cf. Klypin et al. 2002 and Gnedin et al. 2010; see also Binney & Tremaine 2008) and a dark matter component of Navarro-Frenk-White (Navarro et al. 1996) form. The red and green lines assume virial masses of $M_{\text{vir}} = 1 \times 10^{12} M_{\odot}$ and $M_{\text{vir}} = 2 \times 10^{12} M_{\odot}$ respectively, while the solid and dashed lines are for halo concentrations of $c_{\text{vir}} = 20$ and $c_{\text{vir}} = 10$.

An NFW model with a virial mass of $M_{\text{vir}} \sim 10^{12} M_{\odot}$ and a relatively high concentration, $c_{\text{vir}} = 20$ (solid, red line) is favoured by our new constraint on the Galactic potential in the radial range $16 < r/\text{kpc} < 48$. A virial mass of $10^{12} M_{\odot}$ is towards the lower end of independent measurements from local group timing arguments (Li & White 2008) and the kinematics of satellite galaxies Watkins et al. (2010). However, constraints from kinematic stellar halo tracers (e.g. Battaglia et al. 2005; Xue et al. 2008), the local escape speed (Smith et al. 2007) and the orbits of the Magellanic clouds (e.g. Busha et al. 2011) also favour a less massive halo with $M_{\text{vir}} \sim 0.5 - 2 \times 10^{12} M_{\odot}$.

The mass-concentration relation of cosmological simulations (e.g. Macciò et al. 2008) predict a mean concentration of $c_{\text{vir}} \sim 10$ for haloes of mass $10^{12} M_{\odot}$. Thus, the concentration of our favoured dark matter halo seems to be at odds with the predictions of Λ CDM simulations. However, the inferred mass-concentration relation is based on dark matter only simulations. Several authors (e.g. Blumenthal et al. 1986; Mo et al. 1998; Gnedin et al. 2004) have suggested that the influence of baryons at the centre of the halo potential well can lead to an adiabatically contracted dark matter halo (i.e. a more highly concentrated dark matter component). We note that Smith et al. (2007) favour a adiabatically contracted dark matter halo from their local escape velocity constraints. The ‘standard’ dark matter halo of this work is strikingly similar to the solid, red model shown in Fig. 4 with $M_{\text{vir}} = 0.9 \times 10^{12}$ and $c_{\text{vir}} = 24$. Note that the concentration of the favoured model of Battaglia et al. (2005) is also relatively high for their inferred halo mass: $M_{\text{vir}} = 0.8 \times 10^{12}$ and $c_{\text{vir}} = 18$.

4 CONCLUSIONS

We studied the potential of the Milky Way by using BHB stars as halo tracers. We modelled the tracer density as a flattened power-law embedded in a spherically symmetric, power-law gravitational potential. The shape of the tracer velocity distribution is controlled by the constant velocity anisotropy parameter β . We used a maximum likelihood method to derive the potential power-law slope γ and normalisation Φ_0 , in addition to the velocity anisotropy of the tracer population.

By adopting our favoured tracer density model with slope $\alpha = 4.6$ and flattening $q = 0.59$, we find that BHB tracers in the radial range $16 < r/\text{kpc} < 48$ have a radially biased velocity anisotropy with $\beta = 0.5^{+0.08}_{-0.2}$. The agreement of this result with local solar neighbourhood measurements suggests that the velocity anisotropy of stellar halo stars may be constant to a good approximation over a relatively large radial range. We also measure the power-law slope of the overall potential to be $\gamma \sim 0.4$, which lies in-between the isothermal ($\gamma = 0$) and Keplerian ($\gamma = 1$) regimes. This model implies that the total mass within 50 kpc is

$M(50) \sim 4 \times 10^{11} M_{\odot}$, in good agreement with other independent estimates in the literature. Neglecting the flattening of the stellar halo only has a small effect; the velocity anisotropy is less radially biased and the slope of the potential is slightly shallower. However, shallower tracer density profiles – such as the commonly adopted power-law $\alpha = 3.5$ – lead to a lower inferred halo mass and a different circular velocity profile.

For the first time, we have provided a measure of the circular velocity profile of the Galaxy in the Galactocentric radial range $16 \text{ kpc} < r < 48 \text{ kpc}$. Our results suggest that the dark matter potential may be more centrally concentrated than the predictions of dark matter only simulations; this might be a consequence of adiabatic contraction in this inner radial regime.

This work is a useful step towards obtaining a detailed description of the mass profile of our Galaxy. However, further progress requires tighter constraints on the tracer population properties at larger distances ($r > 80 \text{ kpc}$). This presents a daunting task; not only do we suffer from a lack of kinematic tracers at such large distances, but we have very little knowledge of the tracer density profile. Moreover, we have no constraint on the velocity anisotropy as we purely observe the radial velocity component at such distances (i.e. $v_{\text{los}} \sim v_r$). New and future surveys and observational facilities, such as the Large Synoptic Survey Telescope and the planned 30m class of telescopes, will be of vital importance in order to tackle this problem.

ACKNOWLEDGEMENTS

AJD thanks the Science and Technology Facilities Council (STFC) for the award of a studentship, whilst VB acknowledges financial support from the Royal Society. We thank X.X. Xue for kindly providing the SDSS DR8 BHB sample, as well as the referee for helpful comments.

REFERENCES

- Agnello A., Evans N. W., 2012, MNRAS, 422, 1767
- An J. H., Evans N. W., 2006, AJ, 131, 782
- Battaglia G., et al., 2005, MNRAS, 364, 433
- Besla G., Kallivayalil N., Hernquist L., Robertson B., Cox T. J., van der Marel R. P., Alcock C., 2007, ApJ, 668, 949
- Binney J., Tremaine S., 2008, Galactic Dynamics: Second Edition. Princeton University Press
- Blumenthal G. R., Faber S. M., Flores R., Primack J. R., 1986, ApJ, 301, 27
- Bond N. A., et al., 2010, ApJ, 716, 1
- Busha M. T., Marshall P. J., Wechsler R. H., Klypin A., Primack J., 2011, ApJ, 743, 40
- Chen B., et al., 2001, ApJ, 553, 184
- de Bruijne J. H. J., van der Marel R. P., de Zeeuw P. T., 1996, MNRAS, 282, 909
- Deason A. J., Belokurov V., Evans N. W., 2011a, MNRAS, 411, 1480
- Deason A. J., Belokurov V., Evans N. W., 2011b, MNRAS, 416, 2903
- Diemand J., Kuhlen M., Madau P., 2007, ApJ, 667, 859
- Evans N. W., Hafner R. M., de Zeeuw P. T., 1997, MNRAS, 286, 315
- Gnedin O. Y., Brown W. R., Geller M. J., Kenyon S. J., 2010, ApJ, 720, L108

³ Note that smaller scale lengths (e.g. 2 kpc) make little difference to the circular velocity profile in the radial range probed by this work.

- Gnedin O. Y., Kravtsov A. V., Klypin A. A., Nagai D., 2004, *ApJ*, 616, 16
- Jurić M., et al., 2008, *ApJ*, 673, 864
- Kepley A. A., et al., 2007, *AJ*, 134, 1579
- Klypin A., Zhao H., Somerville R. S., 2002, *ApJ*, 573, 597
- Kochanek C. S., 1996, *ApJ*, 457, 228
- Koposov S. E., Rix H.-W., Hogg D. W., 2010, *ApJ*, 712, 260
- Li Y.-S., White S. D. M., 2008, *MNRAS*, 384, 1459
- Lin D. N. C., Lynden-Bell D., 1982, *MNRAS*, 198, 707
- Macciò A. V., Dutton A. A., van den Bosch F. C., 2008, *MNRAS*, 391, 1940
- McMillan P. J., 2011, *MNRAS*, 414, 2446
- McMillan P. J., Binney J. J., 2010, *MNRAS*, 402, 934
- Mo H. J., Mao S., White S. D. M., 1998, *MNRAS*, 295, 319
- Navarro J. F., Frenk C. S., White S. D. M., 1996, *ApJ*, 462, 563
- Navarro J. F., Ludlow A., Springel V., Wang J., Vogelsberger M., White S. D. M., Jenkins A., Frenk C. S., Helmi A., 2010, *MNRAS*, 402, 21
- Newberg H. J., Yanny B., 2006, *Journal of Physics Conference Series*, 47, 195
- Reid M. J., et al., 2009, *ApJ*, 700, 137
- Sakamoto T., Chiba M., Beers T. C., 2003, *A&A*, 397, 899
- Sales L. V., Navarro J. F., Abadi M. G., Steinmetz M., 2007, *MNRAS*, 379, 1464
- Sesar B., Jurić M., Ivezić Ž., 2011, *ApJ*, 731, 4
- Sirko E., et al., 2004, *AJ*, 127, 899
- Smith M. C., et al., 2007, *MNRAS*, 379, 755
- Smith M. C., et al., 2009a, *MNRAS*, 399, 1223
- Smith M. C., Wyn Evans N., An J. H., 2009b, *ApJ*, 698, 1110
- Watkins L. L., Evans N. W., An J. H., 2010, *MNRAS*, 406, 264
- Wilkinson M. I., Evans N. W., 1999, *MNRAS*, 310, 645
- Xue X. X., et al., 2008, *ApJ*, 684, 1143
- Xue X. X., et al., 2011, *ApJ*, 738, 79
- Yanny B., et al., 2000, *ApJ*, 540, 825